

# Final Project, MECH510

Shayan Hoshyari  
Student #: 81382153

December 2015

## Contents

<b>1 The Problem</b>	<b>1</b>
<b>2 Numerical Method</b>	<b>2</b>
<b>3 Results</b>	<b>2</b>
3.1 Correctness of Residual . . . . .	3
3.2 Correctness of Jacobian . . . . .	4
3.3 Validation Case: Stability . . . . .	4
3.4 Solution when $U_{top} = 1$ . . . . .	6
3.5 Sanity check: Symmetry . . . . .	6
3.6 Grid Convergence . . . . .	6
3.7 Effect of parameters $A$ and $\beta$ . . . . .	8
3.8 Solution for $H = 2$ . . . . .	9
3.9 Creation of a Third Main Vortex . . . . .	10
<b>4 Conclusion</b>	<b>12</b>

## 1 The Problem

In this project we will solve for the steady state solution of the two-dimensional, incompressible, laminar Navier-Stokes equations on regular Cartesian grids. Combined with the artificial compressibility method the equations read as:

$$\mathbf{U}_t + \mathbf{F}_x + \mathbf{G}_y = 0$$

The vectors  $\mathbf{U}$ ,  $\mathbf{F}$  and  $\mathbf{G}$  are the unknowns, the flux in the  $x$  direction, and the flux in the  $y$  direction respectively. They are defined as:

$$\mathbf{U} = \begin{bmatrix} p \\ u \\ v \end{bmatrix} \quad \mathbf{F} = \begin{bmatrix} u/\beta - Ap_x\Delta x\Delta y \\ u^2 + p - u_x/\text{Re} \\ uv - v_x/\text{Re} \end{bmatrix} \quad \mathbf{G} = \begin{bmatrix} v/\beta - Ap_y\Delta x\Delta y \\ uv - u_y/\text{Re} \\ v^2 + p - v_y/\text{Re} \end{bmatrix}$$

The Reynolds number is the governing dimensionless number and is shown by  $\text{Re}$ .  $p$  is the pressure, while  $u$  and  $v$  represent the velocities in  $x$  and  $y$  direction respectively.  $\beta$  is the artificial compressibility factor and  $A$  introduces an additional second order error term in the solution in expense of removing pressure oscillations.

The computational domain is a rectangular box with width  $W = 1$  and height  $H$ . Wall boundary conditions are used for all the four sides of the box:

$$p_n = 0, \quad u = U_{\text{wall}}, \quad v = V_{\text{wall}}$$

Finally, the upper wall moves with the speed  $U_{\text{top}}$ , while the other walls are stationary.

## 2 Numerical Method

Solving the Navier-Stokes equations is divided into two main parts: space discretization and time discretization. To discretize the equations in space we use the finite volume method and the second order central interpolation scheme to transform the original PDE into a set of algebraic differential equations:

$$\frac{d\bar{\mathbf{U}}}{dt} = \mathbf{R}(\bar{\mathbf{U}})$$

Where  $\mathbf{R}$  is the flux integral of all cells divided by cell size and  $\bar{\mathbf{U}}$  is the average value of solution for all cells. We are only interested in the steady-state solution  $\mathbf{R}(\bar{\mathbf{U}}) = \mathbf{0}$ . However, we will take advantage of the transient form of the equations and use a combination of the Implicit Euler method and the Newton's method to find the steady state solution. The Implicit Euler method transforms the set of algebraic differential equations into a system of nonlinear equations (subscript  $n$  means at time step  $n$ ):

$$\bar{\mathbf{U}}_{n+1} = \bar{\mathbf{U}}_n + \Delta t \mathbf{R}(\bar{\mathbf{U}}_{n+1})$$

As we are not interested in the transient solution, instead of solving this system exactly we will only perform one Newton iteration on it:

$$\left( \frac{\mathbf{I}}{\Delta t} - \frac{\partial \mathbf{R}}{\partial \bar{\mathbf{U}}}(\bar{\mathbf{U}}_n) \right) \delta \mathbf{U} = \mathbf{R}(\bar{\mathbf{U}}_n)$$

We solve this system using the approximate factorization method. Finally we update the solution, optionally using over-relaxation:

$$\bar{\mathbf{U}}_{n+1} = \bar{\mathbf{U}}_n + \omega \delta \mathbf{U}$$

This process is continued until certain criteria are met, e.g.,  $\|\delta \mathbf{U}\| < \epsilon$  where  $\epsilon$  is a very small number.

## 3 Results

In this section the results for each part of the project are presented.

### 3.1 Correctness of Residual

The method of manufactured solutions will be used to verify the correctness of the flux integral code. The computational domain is defined as the region:  $[0 \ 1] \times [0 \ 1]$ . The average values of unknowns for internal cells are found using the midpoint integration rule and the formula:

$$\mathbf{U} = \begin{bmatrix} p \\ u \\ v \end{bmatrix} = \begin{bmatrix} \cos(\pi x) \cos(\pi y) \\ \sin(\pi x) \sin(2\pi y) \\ \sin(2\pi x) \sin(\pi y) \end{bmatrix}$$

Table 1:  $L_2$  Error norms of flux integral for two different meshes.

Mesh size	All terms	$p$ flux	$u$ flux	$v$ flux
$20 \times 20$	$4.142 \times 10^{-2}$	$1.198 \times 10^{-2}$	$5.002 \times 10^{-2}$	$5.002 \times 10^{-2}$
$40 \times 40$	$1.042 \times 10^{-2}$	$0.299 \times 10^{-2}$	$1.258 \times 10^{-2}$	$1.258 \times 10^{-2}$

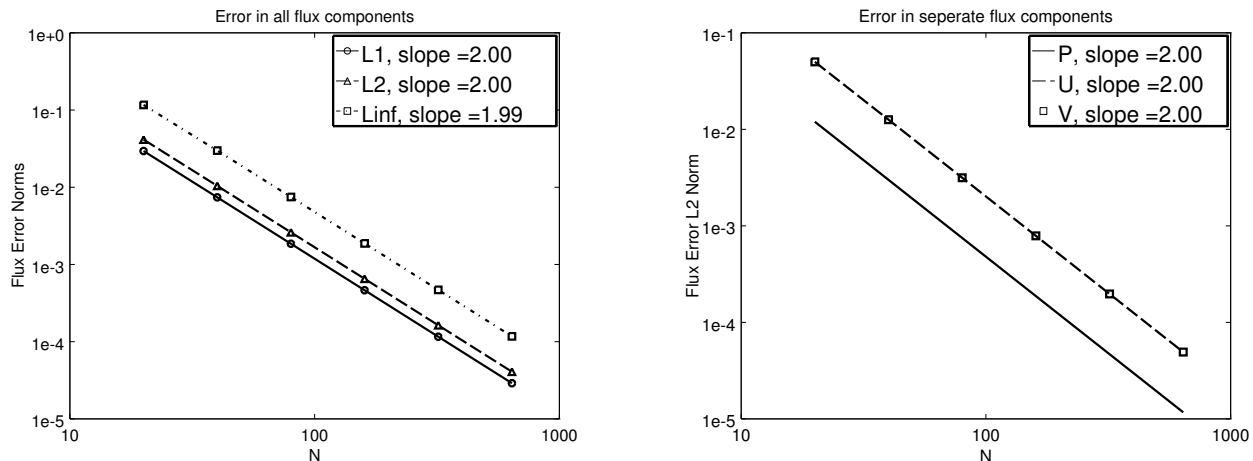


Figure 1: The left figure shows the norms of the error in all fluxes all together, while the right figure shows the  $L_2$  norm of the error in each flux separately. The horizontal axis shows the number of control volumes in each direction and the slopes are found using least square curve fitting.

The average solution values for the ghost cells are found using the boundary conditions ( $U_{\text{top}} = 0$ ). Then the values  $R_{ij}$  will be calculated and compared with their exact counterparts. Due to their huge size the exact values are not given here. However, they can be found by inserting the known values of  $p$ ,  $u$  and  $v$  into the definitions of  $\mathbf{F}$  and  $\mathbf{G}$ .

In Figure 1 the error norms of the flux integral (both all together and separately) are shown for a set of refined meshes, while  $\text{Re}=10$ ,  $\beta = 1$  and  $A = 0$ . To study the behavior of flux integral error more closely, Table 1 shows the  $L_2$  error norms of the flux integral for the  $20 \times 20$  and  $40 \times 40$  meshes. The fact that all error norms get four times smaller when  $\Delta x$  and  $\Delta y$  are halved verifies that the flux integral is coded correctly. It is also interesting that the error norms for the velocity fluxes are almost identical.

### 3.2 Correctness of Jacobian

To verify the Jacobian code, the following approximation will be used:

$$\left(\frac{\partial \mathbf{R}}{\partial \bar{\mathbf{U}}}\right) \delta \mathbf{U} \approx \mathbf{R}(\bar{\mathbf{U}} + \delta \mathbf{U}) - \mathbf{R}(\bar{\mathbf{U}})$$

Generally,  $\delta \mathbf{U}$  can be any vector with a small magnitude. However, for simplicity, we set it to be:

$$\delta \mathbf{U}_{ij} = \begin{cases} 10^{-6} \mathbf{I} & i = j = c \\ 0 & \text{otherwise} \end{cases}$$

As we are using the central method to interpolate the solution at control volume faces, we know that the only fluxes that are going to change are  $\mathbf{R}_{c-1,c}$ ,  $\mathbf{R}_{c+1,c}$ ,  $\mathbf{R}_{c,c+1}$ , and  $\mathbf{R}_{c,c-1}$ .

In Table 2 the difference in the two methods to approximate the change in flux integral is shown for  $\mathbf{R}_{c-1,c}$ ,  $\mathbf{R}_{c+1,c}$ ,  $\mathbf{R}_{c,c+1}$ , and  $\mathbf{R}_{c,c-1}$ , when the values of  $\bar{\mathbf{U}}$  and  $\text{Re}$  are the same as Section 3.1,  $c = 10$ , and

Table 2: Differences in approximating the change in flux integral using the Jacobian or the flux integral itself. The initial solution values are the same as Section 3.1, and the solution at cell  $i = j = 10$  is perturbed by an amount of  $10^{-6}$ .

Cell	$p$ flux	$u$ flux	$v$ flux
(10, 9)	$-5.09 \times 10^{-16}$	$-4.99 \times 10^{-12}$	$-4.99 \times 10^{-12}$
(9, 10)	$-1.39 \times 10^{-15}$	$-5.00 \times 10^{-12}$	$-4.99 \times 10^{-12}$
(10, 10)	$8.88 \times 10^{-16}$	$-7.11 \times 10^{-16}$	$-7.66 \times 10^{-16}$
(10, 11)	$6.55 \times 10^{-17}$	$5.00 \times 10^{-12}$	$4.99 \times 10^{-12}$
(11, 10)	$6.55 \times 10^{-17}$	$4.99 \times 10^{-12}$	$4.99 \times 10^{-12}$

a  $20 \times 20$  mesh is used. Being smaller than  $10^{-10}$ , these small differences verify the correctness of the Jacobian. It is also worth mentioning that the errors for the  $p$  flux are the smallest because this flux is linear in  $u$  and  $v$ , so the approximation is actually exact and the difference is due to computer round off errors.

### 3.3 Validation Case: Stability

In this section the equations will be solved for  $W = H = 1$  and  $U_{top} = 0$  on a  $20 \times 20$  grid. It is expected that the solution converge to the value of zero everywhere. The values introduced in Section 3.1 are used as initial conditions (except that the origin is at the top left corner of the box instead of the lower left corner). Other parameters are set to  $A = 0$ ,  $\beta = 1$ ,  $Re = 100$  and  $\Delta t = 0.05$ . To study the effect of over-relaxation three different values for  $\omega$  will be tested.

Figure 2 shows the  $L_2$  norm of change in solution for the first 200 iterations. It is observed that over-relaxing the solution enhances convergence after a certain amount of iterations (50 in this case). The  $L_2$  norm of change in all variables is monotonically decreasing. However, individual variables demonstrate an oscillatory convergence history. In Section 3.4 it will be shown that a smart choice of time step can prevent this behavior and enhance convergence considerably. Fortunately, these oscillation begin to damp after a few hundred iterations and the convergence history becomes completely monotonic (not shown in the graph).

### 3.4 Solution when $U_{top} = 1$

In this section the problem will be solved for  $U_{top} = 1$  on a  $20 \times 20$  grid. Optimum values of  $\Delta t = 0.27$  and  $\omega = 1.3$  are found experimentally and will be used. We iterate until the largest  $L_2$  norm in solution gets smaller than  $10^{-6}$ . Other parameters have the same value as Section 3.3.

Figure 3 shows the contour plots of the pressure. As  $A$  is chosen to be zero the solution converges to an oscillatory pressure field. However, Paraview's interpolation mechanism does not show this phenomenon in the plot. The figure also shows that the pressure is unbounded at the top right and left corners, where it has a maximum and minimum respectively. There is also a local minimum for the pressure field somewhere around (0.7, 0.7).

Figure 4 shows the convergence history. The choice of  $\Delta t$  in this case has improved convergence immensely. The oscillatory behavior of  $L_2$  norm in change of solution is gone and the number of iterations is four times smaller compared to  $\Delta t = 0.05$ . My experiments in using different values of  $\Delta t$  showed that there is a range of  $\Delta t$  for which the solution converges, with the optimum time step somewhere in between. For  $\Delta t = 0.05$  the solution always converges even for 300 meshes per unit length. However, the maximum and

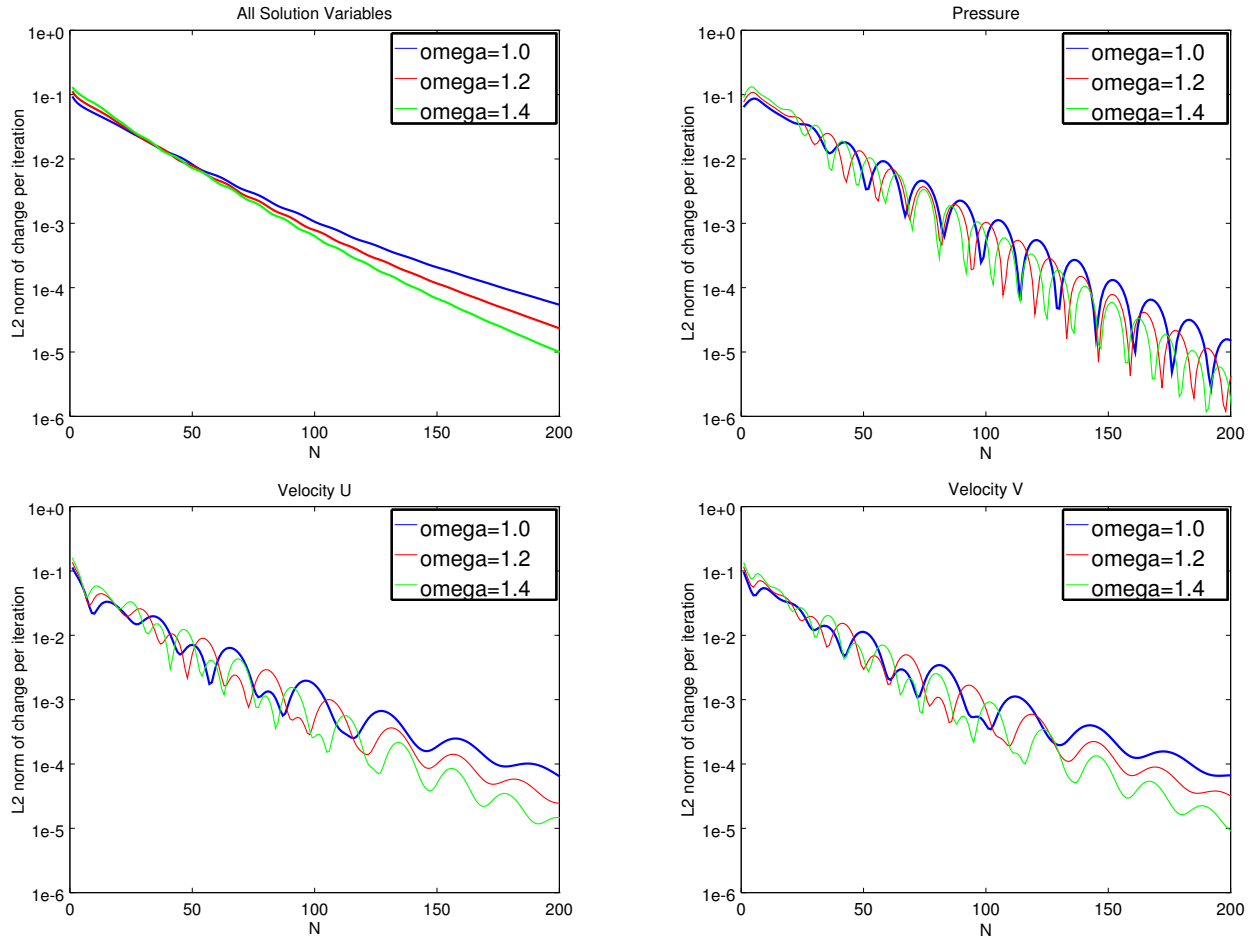


Figure 2: Convergence history for  $U_{top} = 0$ . Different values of  $\omega$  are used to study the effect of over-relaxation.

Table 3: The order of convergence obtained for the velocity profile on the vertical symmetry line, when  $Re=100$ ,  $H=1$  and  $U=1$ . Two series of meshes are used, and the analysis is carried out using the  $L_1$ ,  $L_2$  and  $L_\infty$  norm of the change in the profile.

Meshes	$L_1$	$L_2$	$L_\infty$
$10 \times 10, 20 \times 20, 40 \times 40$	1.45	1.70	2.43
$20 \times 20, 40 \times 40, 80 \times 80$	1.90	1.77	1.41

optimum time steps get smaller as the mesh gets finer. For example, the optimum time step is around 0.27 and 0.10 for  $20 \times 20$  and  $180 \times 180$  meshes respectively.

Figure 5 shows the  $u$  velocity on the line  $x=0.5$ . In this graph the value of  $u$  at  $y=0,1$  is obtained using the exact enforced boundary conditions, whereas other values of  $u$  are obtained by interpolating from the average control volume values of  $u$  from the two cells adjacent to the line  $x=0.5$ .

### 3.5 Sanity check: Symmetry

In this section the problem will be solved with the same parameters as Section 3.4, except for  $U_{top}=-1$ . Because of symmetry it is expected that the value  $u_{U_{top}=-1}(1-x,y)+u_{U_{top}=1}(x,y)$  be very small throughout the domain. Figure 6 shows this property for two different cases: when the initial conditions are chosen like those of Section 3.1, and when the initial conditions are zero for all unknowns. Interestingly, when the nonzero initial conditions are used, the deviation from symmetry follows a pattern similar to the initial conditions. On the other hand, for the zero initial conditions the deviation does not follow any pattern and is even smaller by a factor of  $10^{-10}$ .

### 3.6 Grid Convergence

The same problem from Section 3.4 will be solved on a series of refined meshes ( $10 \times 10, 20 \times 20, 40 \times 40$  and  $80 \times 80$ ) to study grid convergence. I will use Richardson Extrapolation on the  $u$  velocity profile on the vertical symmetry line. Figure 7 shows the  $u$  velocity on this line for all the meshes. The solution changes considerably from the  $10 \times 10$  mesh to the  $20 \times 20$ , while the change for further refinements is relatively subtle.

To investigate grid convergence further, I will compute the norm of the change in the velocity from the coarse to the refined mesh for each case. A simple interpolation was needed to find the solution at the same points for the two different meshes. Figure 8 shows these norms. Then I will use Richardson Extrapolation to find order of convergence according to the formula:

$$p = \log_2 \left( \frac{\|u_1 - u_2\|}{\|u_2 - u_3\|} \right)$$

where 1 and 3 stand for the coarsest and finest meshes respectively. Table 3 shows the order of convergence found using different norm types and two different sets of meshes. As we are using a second order method to solve a non-linear system of equations, we expect the order to be somewhere between one and two. The fact that for the first series of meshes the  $L_\infty$  based order of convergence is bigger than two, suggests that these meshes might not be fine enough and the change in solution has not approached its asymptotic behavior yet. The orders of convergence for the second series of meshes are all in the acceptable range, and demonstrate grid convergence.

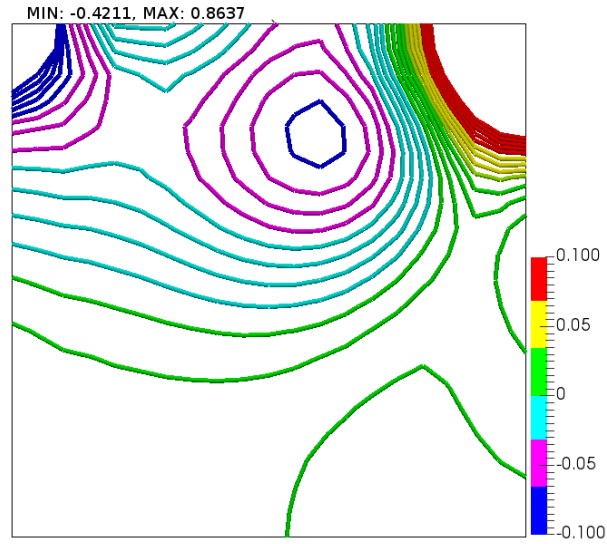


Figure 3: Pressure contours for  $U_{\text{top}} = 1$ ,  $H = 1$  and a  $20 \times 20$  grid. As the pressure is unbounded at the top corners the contours are plotted for  $|p| < 0.1$ , and the numerical values of the pressure at the corners are presented separately.

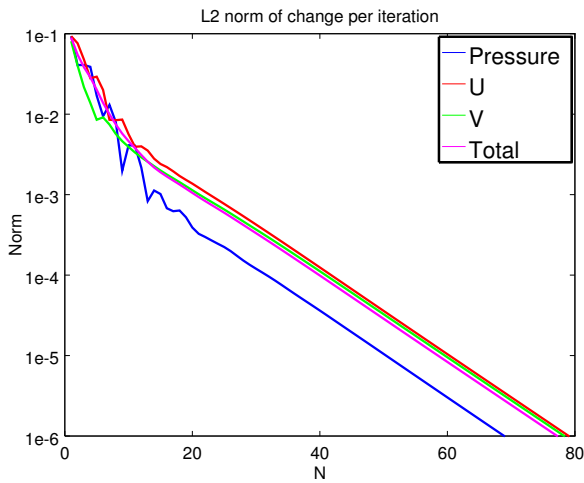


Figure 4: Convergence history for  $U_{\text{top}} = 1$ ,  $H = 1$  and a  $20 \times 20$  grid.

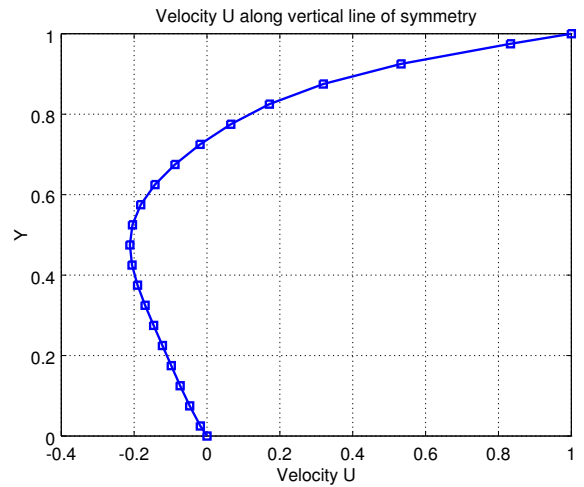


Figure 5:  $u$  velocity on the vertical symmetry line for  $U_{\text{top}} = 1$ ,  $H = 1$  and a  $20 \times 20$  grid.

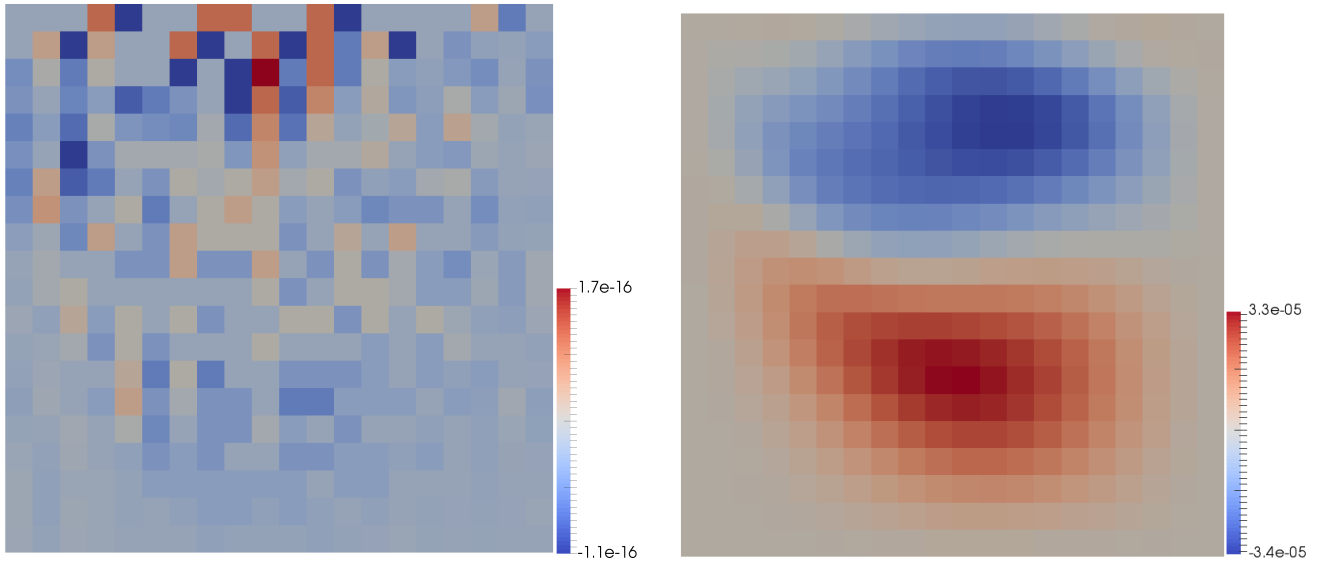


Figure 6: The value of  $u_{U_{top}=-1}(1-x, y) + u_{U_{top}=1}(x, y)$  for a  $20 \times 20$  mesh and  $Re=100$ . In the left figure zero initial conditions are used for all the solution variables, whereas on the right figure the initial conditions were chosen similar to those of Section 3.1.

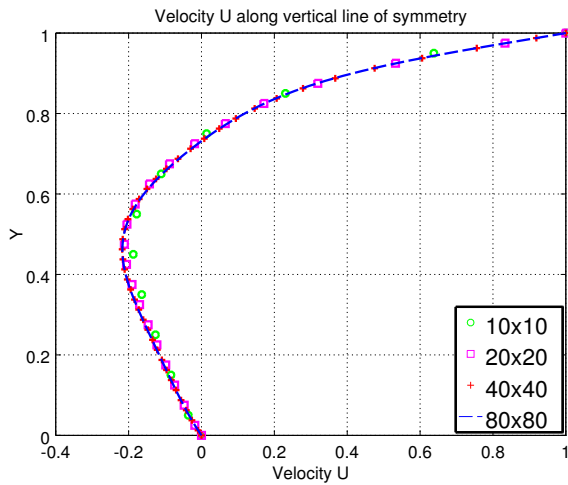


Figure 7: The  $u$  velocity on the vertical symmetry line for various mesh sizes.

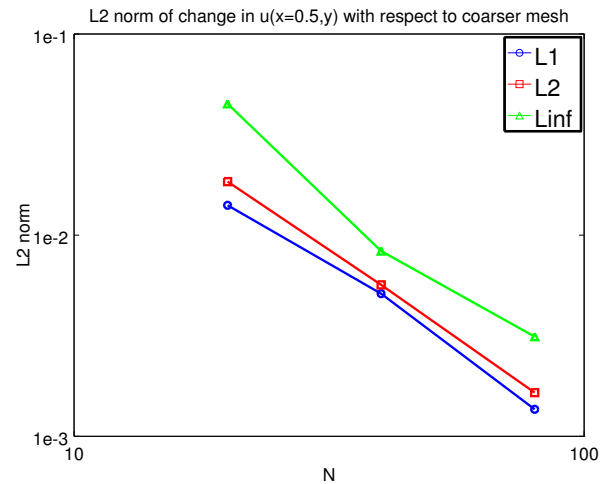


Figure 8: The norms of change in the velocity profile  $u(x = 0.5, y)$ , with respect to mesh refinement.



Figure 9: Pressure distribution on  $y = 0.5$  for different values of  $A$ .

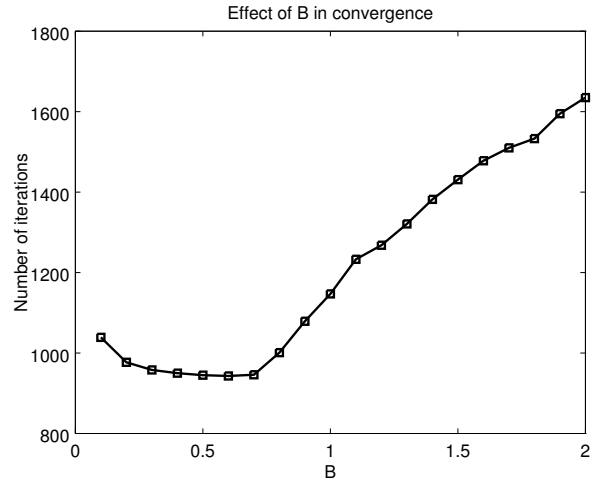


Figure 10: Number of iterations required for convergence for different values of  $\beta$ .

### 3.7 Effect of parameters $A$ and $\beta$

In this section I will study the effect of  $A$  and  $\beta$ . The problem will be solved on a  $40 \times 40$  mesh, with  $\text{Re} = 100$ ,  $\omega = 1$  and  $\Delta t = 0.05$ . The convergence criterion is that the  $L_2$  norm of the change in all unknowns falls below  $10^{-13}$ .

Figure 9 shows the pressure distribution on the line  $y = 0.5$  when  $\beta = 1$ . The value  $A = 0.1$  reduces the oscillations, but they are still present. The value  $A = 0.6$  seems to be a good choice, as it removes most of the oscillations. Increasing  $A$  further does not seem to have any effect on the solution. Not only does a good choice for  $A$  remove pressure oscillations, but it also improves convergence, reducing number of iterations from 3000 to 1000.

Figure 10 shows the number of iterations required for convergence when  $A = 0.6$ . Apparently,  $\beta = 0.6$  improves the convergence a little bit, although this improvement is subtle compared to the effect of  $\Delta t$ ,  $\omega$  or  $A$ .

### 3.8 Solution for $H = 2$

I will solve the problem for  $H = 2$ ,  $\text{Re} = 200$ ,  $A = 0.6$  and  $\epsilon = 10^{-13}$  then I will estimate the center location and the strength of the vortices. Figure 11 shows the streamlines obtained using a  $180 \times 360$  mesh for this case, verifying that there are four vortices present. The stream function is found by integrating the  $v$  velocity on horizontal lines using the trapezoidal integration rule and the initial condition of  $\psi = 0$  on the left wall.

To find the strength of the vortices, I will integrate the vorticity in the area corresponding to each vortex and then divide it by the area:

$$\text{strength} = \frac{1}{A} \left| \int_A (v_x - u_y) dA \right|$$

The regions are identified, using the stream function. Because no fluid crosses the vortex boundaries,  $\psi$  should be constant on them. As the boundaries are connected to the walls, the value of  $\psi$  on the vortex boundaries is zero. Figure 11 shows that  $\psi$  also changes sign from one vortex to another, so we can use it to identify which cell belongs to which vortex.

Table 4: The center location and the strength of the vortices, and their error estimates for  $H = 2$ .

	vortex 1			vortex 2		
	$x_0$	$y_0$	strength	$x_0$	$y_0$	strength
Value for $80 \times 160$	0.599132	1.661717	1.0756e+00	0.512717	0.779242	2.8117e-02
Value for $120 \times 240$	0.598578	1.661251	1.0781e+00	0.511910	0.781485	2.8389e-02
Value for $180 \times 360$	0.598308	1.661127	1.0787e+00	0.511544	0.782432	2.8438e-02
Extrapolated Value	0.598051	1.661082	1.0789e+00	0.511242	0.783124	2.8448e-02
Order of Convergence	1.77	3.25	3.55	1.95	2.12	4.22
Estimated Error	0.042934	0.002727	0.017510	0.059202	0.088366	0.037848
	vortex 3			vortex 4		
	$x_0$	$y_0$	strength	$x_0$	$y_0$	strength
Value for $80 \times 160$	0.960495	0.036851	4.0825e-04	0.039849	0.037823	5.2809e-04
Value for $120 \times 240$	0.962505	0.037983	2.8740e-04	0.038071	0.038651	2.7866e-04
Value for $180 \times 360$	0.962411	0.037348	2.3729e-04	0.038047	0.038535	2.2377e-04
Extrapolated Value	0.962406	0.036534	2.0181e-04	0.038046	0.038516	2.0827e-04
Order of Convergence	7.55	1.42	2.17	10.57	4.84	3.73
Estimated Error	0.000480	2.226166	17.580681	0.000891	0.049124	7.437678

To find the vortex centers, I used Paraview’s glyph filter to plot the velocity at the center of all the cells. As I already knew the approximate location of the centers from the streamlines, I searched there to find:

- Four cells whose velocity is turning around the common vertex. In this case the reference point is the common vertex.
- A cell with the velocity of its adjacent cells turning around it. In this case the reference point will be the center of the middle cell.

Then I did a reconstruction of velocities around the reference point and solved for  $u = v = 0$  to find the vortex center. The best reference point is the one that gives the smallest  $x - x|_{\text{ref}}$  and  $y - y|_{\text{ref}}$ .

$$\begin{bmatrix} u_x|_{\text{ref}} & u_y|_{\text{ref}} \\ v_x|_{\text{ref}} & v_y|_{\text{ref}} \end{bmatrix} \begin{bmatrix} x - x|_{\text{ref}} \\ y - y|_{\text{ref}} \end{bmatrix} = \begin{bmatrix} -u|_{\text{ref}} \\ -v|_{\text{ref}} \end{bmatrix}$$

Table 4 shows the results obtained for each vortex. The upper, middle, lower right and lower left vortices are numbered 1, 2, 3 and 4 respectively. Judging by the strength value of vortex 3 and 4, it seems that the  $80 \times 160$  mesh is too coarse for this case. Unfortunately, I can not afford finer meshes than  $180 \times 360$ , so I am going to stick with the  $80 \times 160$  mesh for error estimation. The cases with the order of convergence higher than two might also mean that the meshes are not fine enough.

### 3.9 Creation of a Third Main Vortex

As the height of the box increases at fixed Reynolds number, the flow pattern changes. Vortices in the bottom corners of the box grow in size until eventually they merge to form a third vortex. Using the same parameters as Section 3.8, I found the height at which the two corner vortices have merged into a single vortex, to be  $2.79 \pm 0.01$ .

Figure 12 shows the stream lines for this case when  $\Delta x = \Delta y = \frac{1}{120}$ . We can see that there truly are exactly three closed flow loops. Figure 12 confirms that the fourth vortex is still present for  $H = 2.78$ . I also obtained the same results for  $\Delta x = \Delta y = \frac{1}{180}$  to show that the results are not grid dependent.

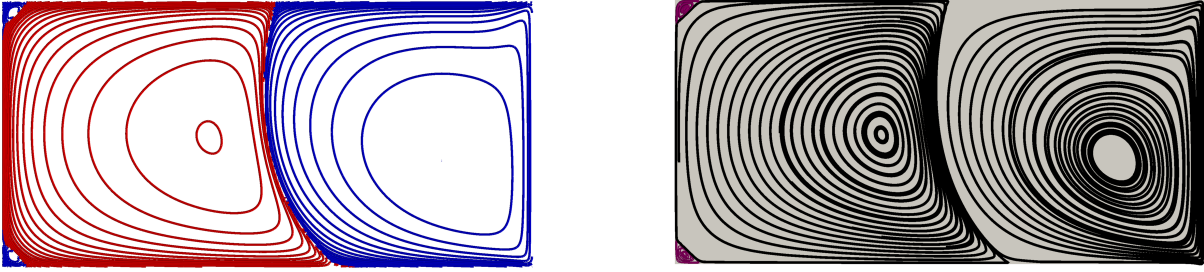


Figure 11: The streamlines for the case  $H = 2$ . The left figure shows the streamlines found using the stream function and the regions where this function changes sign. The right figure shows the streamlines found using Paraview's stream tracer filter, which agree with the stream function results.

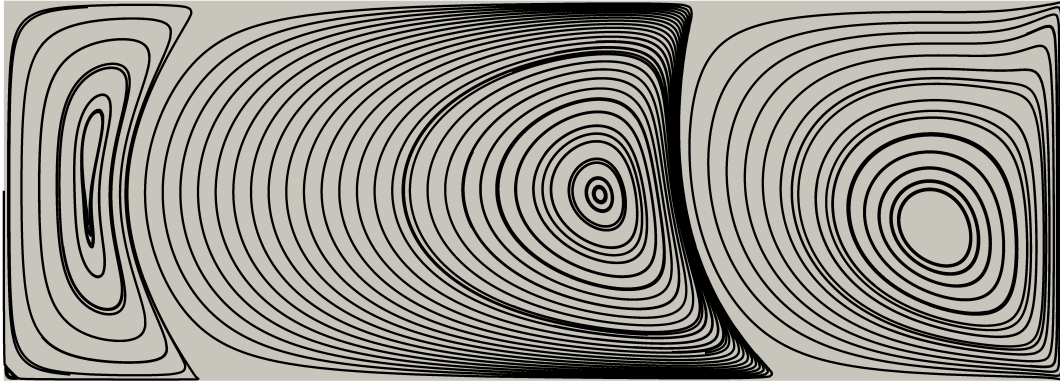


Figure 12: The stream lines for  $H = 2.79$ . It is clear that three main vortices are present in this case.

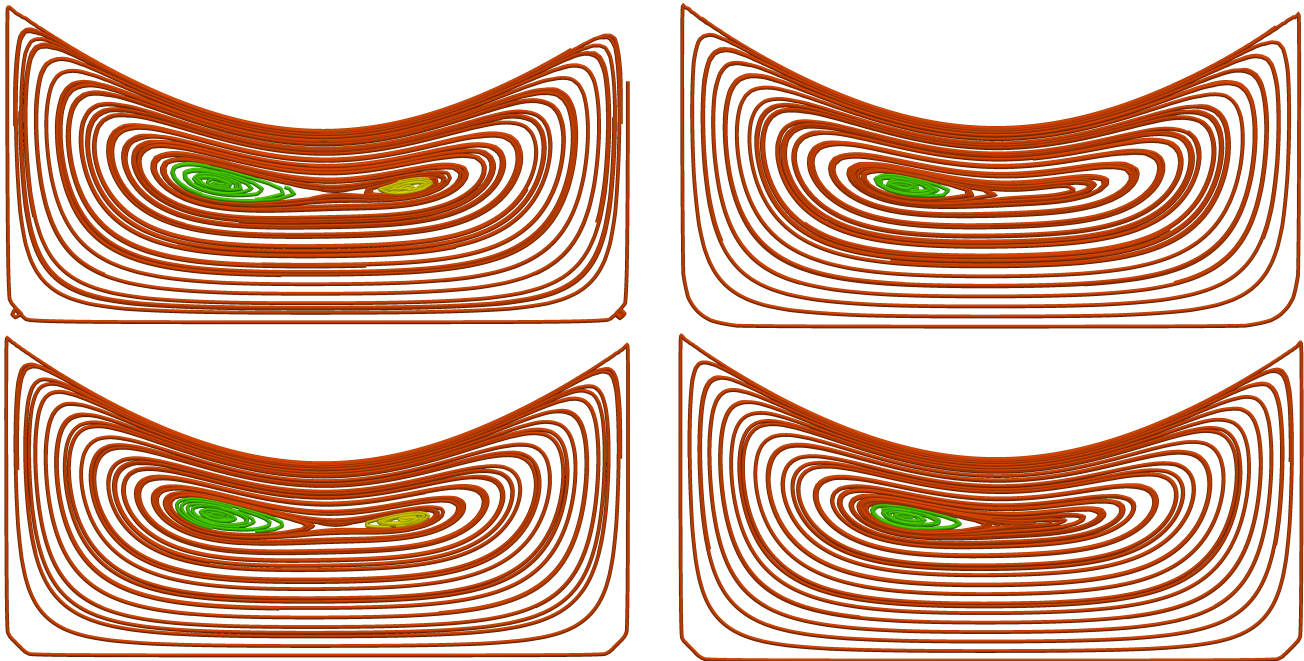


Figure 13: Merging of the two lower vortices. The stream lines on the left are obtained for  $H = 2.79$  and the stream lines on the right are obtained for  $H = 2.78$ . The upper and lower figures correspond to  $\Delta x = \Delta y = \frac{1}{120}$  and  $\Delta x = \Delta y = \frac{1}{180}$  respectively.

## 4 Conclusion

In this assignment the incompressible laminar Navier-Stokes equations were solved using the finite volume method. The fluxes were evaluated using the central approximation scheme while the temporal discretization was done using the Implicit Euler method. The pressure decoupling was handled using the artificial compressibility method.

Firstly, the flux integral was verified to be second order accurate. Then the Jacobian was verified by perturbing the solution and predicting the change in flux integral using the Jacobian. Several other tests were consequently performed to verify the correctness of the numerical method.

Finally, the vortex patterns of the flow in a box with a moving top were studied. The centers of the vortices were found using interpolation, while their strength was evaluated using the stream function and the vorticity.